Hyperbolic Weyl Point in Reciprocal Chiral Metamaterials

Meng Xiao,[1] Qian Lin,[2] and Shanhui Fan[1,*]
[1]Department of Electrical Engineering, and Ginzton Laboratory, Stanford University, Stanford, California 94305, USA
[2]Department of Applied Physics, Stanford University, Stanford, California 94305, USA
(Received 2 April 2016; published 27 July 2016)

We report the existence of Weyl points in a class of noncentral symmetric metamaterials, which has time reversal symmetry, but does not have inversion symmetry due to chiral coupling between electric and magnetic fields. This class of metamaterial exhibits either type-I or type-II Weyl points depending on its nonlocal response. We also provide a physical realization of such metamaterial consisting of an array of metal wires in the shape of elliptical helices which exhibits type-II Weyl points.

DOI: 10.1103/PhysRevLett.117.057401

A Weyl point is a topologically singular point in three-dimensional wave vector space. Initially studied in electronic systems [1–10], in recent years the physics of Weyl points has also been studied in classical wave systems such as electromagnetic [11–16] and acoustic systems [17,18]. Compared with the electronic systems, in classical wave systems one has more flexible control of the geometry, and the coherent transport properties are easier to measure due to the lack of electron-electron scattering. Therefore, the classical wave systems complement the electronic systems in the demonstrations of various signatures of the Weyl points. In addition to the fundamental interest, the use of Weyl points may also lead to new capabilities for manipulating the propagation of electromagnetic and acoustic waves.

Recently it was noted that here are two types of Weyl points, type-I and type-II, both are topologically nontrivial but exhibit very different physical properties [10,19]. Up to now, there has not been any exploration of type-II Weyl points in the electromagnetic systems. Here we report the existence of Weyl points in a class of noncentral symmetric electromagnetic metamaterial which preserves time reversal symmetry. The breaking of inversion symmetry is achieved through chiral coupling between electric and magnetic fields. This class of metamaterial exhibits either type-I or type-II Weyl points depending on its nonlocal response [20,21]. We also provide a physical realization of such metamaterial consisting of an array of metal wires in the shape of elliptical helices which exhibits type-II Weyl points.

The simplest model Hamiltonian which exhibits both types of Weyl points has the form $H = \tau k_z \mathbf{I} + k_x\sigma_x + k_y\sigma_y + k_z\sigma_z$ [10], where k_x, k_y, and k_z are the wave vectors along the x, y, and z axes, respectively, σ_x, σ_y, and σ_z are the Pauli matrices, $\mathbf{I}$ is a 2×2 identity matrix and τ is a real constant. In this model, the group velocities of the two bands along the z direction are $\tau+1$ and $\tau-1$, respectively, whereas along either the x or y directions, the group velocities for the two bands are $+1$ and -1, respectively. When $\tau \in (-1, 1)$, the Hamiltonian exhibits a type-I Weyl point at $\vec{k}=\vec{0}$. The constant frequency surface around $\vec{k}=\vec{0}$ is an ellipsoid. Thus one can also refer to such a Weyl point as an elliptical Weyl point. On the other hand, when $\tau \notin [-1, 1]$, the model Hamiltonian exhibits a type-II Weyl point. The constant frequency surface is now a hyperboloid. Therefore, we will also refer to such type-II Weyl points as hyperbolic Weyl points. Both types of Weyl points are topologically nontrivial, but they exhibit very different physical properties. For example, while the density of state is zero at a type-I Weyl point, at a type-II Weyl point, the density of state in fact diverges for this model, similar to hyperbolic metamaterials [22], and can be rather large in the physical realization of this model [10].

Here we report a class of electromagnetic metamaterial that exhibits type-II Weyl points in the homogenization limit. None of the previous works on Weyl points in classical wave systems have reported the observation of a type-II Weyl point. In addition, most of the previous works concerning Weyl points in classical wave systems utilize either photonic or phononic crystals, where the periodicity plays a significant role. The exploration of topological properties in metamaterials as described by homogeneous effective material parameters [23,24] is of fundamental interest since the wave vector space of such metamaterials is noncompact, which is in contrast with the wave vector space of periodic systems which is always topologically compact. As a result, there are significant qualitative differences between the topological properties of metamaterials and photonic crystals as we will discuss in this paper.

Since the Berry curvature vanishes in systems that possess both time reversal and inversion symmetries [11], one needs to break either time-reversal or inversion symmetries to construct a topologically nontrivial object such as a Weyl point. While Refs. [23,24] considered topologically nontrivial metamaterials, their system did not exhibit Weyl points. The existence of Weyl points in homogeneous materials without time-reversal symmetry

has been reported very recently [16]. However, the system in Ref. [16] requires magneto-optical effects under a large static magnetic field, which is challenging to demonstrate experimentally. In this work, we show that Weyl points can be achieved in reciprocal metamaterials where the inversion symmetry is broken with chiral coupling between electric and magnetic fields. And we provide a physical construction of such metamaterials with an array of helix structure that should be relatively straightforward to construct experimentally.

A Weyl point in homogeneous material.—To construct a metamaterial supporting a Weyl point we start with a nonmagnetic ($\mu_r = 1$) anisotropic homogeneous material. The relative permittivity of this material is given by $\overleftrightarrow{\varepsilon}_r = \mathrm{diag}(\varepsilon_t, \varepsilon_t, \varepsilon_z)$, where $\varepsilon_z = 1 - \omega_p^2/\omega^2$ possesses Drude's dispersion. Along the z direction, the system supports three propagating modes, one of which is longitudinal and the other two are transverse. The longitudinal mode is given by $\varepsilon_z = 0$, and hence the dispersion relation of this mode is flat with frequency of the mode fixed at $\omega = \omega_p$ independent of the wave vector k_z along the z direction. The two transverse modes, having their electric field in the xy plane, are influenced only by the permittivity of the transverse directions, i.e., ε_t. Since in this case the system is isotropic along the transverse directions, these two transverse modes are degenerate with their dispersion relation given by $\omega = ck_z/\sqrt{\varepsilon_t}$, where c is the speed of light in vacuum. The dispersion relations of these three modes are shown in Fig. 1(a). They intersect at $k_z = k_c = \omega_p\sqrt{\varepsilon_t}/c$. Therefore, the photon bands are threefold degenerate at $k = (0, 0, k_c)$. Figure 1(b) shows the dispersion relation in the k_x-k_y plane at $k_z = k_c$. Two of the three bands form a conical dispersion around the origin. There is also an additional band, which is quadratic in k_x and k_y, passing through the conical point.

Since a Weyl point is twofold degenerate, we first need to break this triple degeneracy. Here we introduce anisotropy into the relative permittivity by setting

$$\overleftrightarrow{\varepsilon}_r = \mathrm{diag}\{\varepsilon_x, \varepsilon_y, \varepsilon_z\}, \tag{1}$$

where, without loss of generality, we assume $\varepsilon_x > \varepsilon_y$. Along the z axis, the dispersion relation of the two transverse modes becomes (see Supplemental Material S-I [25])

$$\omega = ck_z/\sqrt{\varepsilon_x}, \qquad \omega = ck_z/\sqrt{\varepsilon_y}, \tag{2}$$

as shown schematically in Fig. 1(c). For subsequent discussion we refer to these two bands as bands 1 and 2, respectively. Band 1 thus has a lower frequency compared with band 2 at a given k_z. We refer to the longitudinal mode as band 3. By introducing the anisotropy, the triply degenerate point in the isotropic case now breaks into two linear crossing points. Consider the crossing point between bands 1 and 3. We use k_c to represent the value of k_z at this crossing point. Figure 1(d) shows the dispersion relation in the k_x-k_y plane at $k_z = k_c$. The dispersion is linear along the x direction while quadratic along the y direction. While we have created a twofold degenerate crossing point, this point is not a Weyl point. (The dispersion of a Weyl point is linear along all the directions.) This is expected, since the structure has both time-reversal and inversion symmetry.

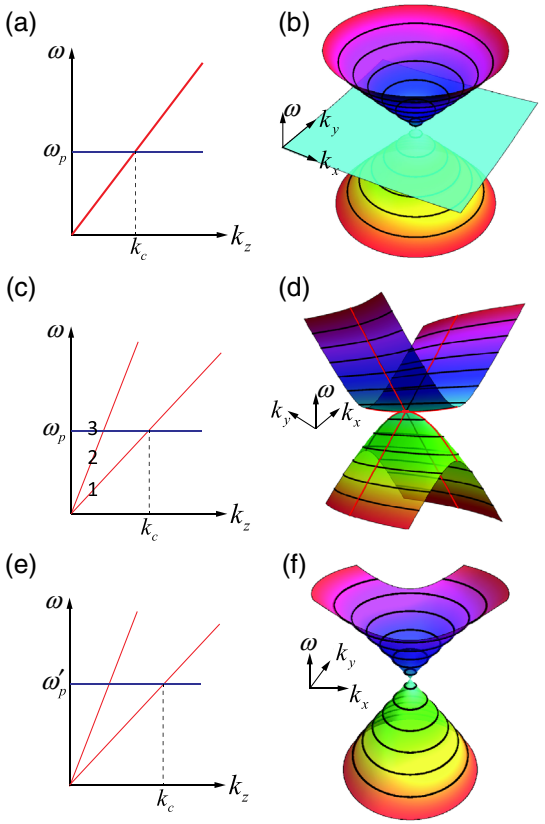

FIG. 1. (a) The dispersion along the z direction of a system with the relative permittivity given by $\overleftrightarrow{\varepsilon} = \mathrm{diag}(\varepsilon_t, \varepsilon_t, \varepsilon_z)$, where $\varepsilon_z = 1 - \omega^2/\omega_p^2$. The bold red line represents the dispersions of two degenerate transverse modes, and the blue horizontal line represents the dispersion of the longitudinal mode. k_c labels the value of k_z at the crossing point. (b) The dispersion in the k_x-k_y plane at $k_z = k_c$. (c) When anisotropy is introduced and $\overleftrightarrow{\varepsilon} = \mathrm{diag}(\varepsilon_x, \varepsilon_y, \varepsilon_z)$, where $\varepsilon_x \neq \varepsilon_y$, the degeneracy between two transverse modes in (a) lifted. (d) The dispersion around one of the crossing points in (c) at $k_z = k_c$. The dispersion is linear along the x direction and quadratic along the y direction. (e) The introducing of chiral coupling along the z direction shifts the frequency of the longitudinal mode. (f) The dispersion around the crossing point in (e) at $k_z = k_c$. (e) and (f) The dispersion is linear along all the directions indicating the crossing point is a Weyl point. Band numbers are labeled in (c). The parameters used are $\omega_p = 1$, $\varepsilon_z = 1 - \omega_p^2/\omega^2$, and $\varepsilon_t = 1.8$ for (b); $\omega_p = 1$, $\varepsilon_z = 1 - \omega_p^2/\omega^2$, $\varepsilon_x = 2$, and $\varepsilon_y = 1.7$ for (d); $\omega'_p = 1$, $\varepsilon_x = 2$, $\varepsilon_y = 1.7$, $\varepsilon_z = 1 - \omega_p'^2/\omega^2 + \gamma_{zz}^2$, and $\gamma_{zz} = 0.8$ for (f).

We break the inversion symmetry by introducing a chiral coupling term between the z components of the electric and magnetic fields [33–34]. The constitutive relation becomes

$$\begin{pmatrix} \vec{D} \\ \vec{B} \end{pmatrix} = \begin{pmatrix} \varepsilon_0 \overleftrightarrow{\varepsilon}_r & i\sqrt{\varepsilon_0\mu_0}\overleftrightarrow{\gamma} \\ -i\sqrt{\varepsilon_0\mu_0}\overleftrightarrow{\gamma} & \mu_0 \end{pmatrix} \begin{pmatrix} \vec{E} \\ \vec{H} \end{pmatrix}, \quad (3)$$

where ε_0 and μ_0 are the permittivity and permeability of the vacuum, respectively, $\overleftrightarrow{\varepsilon}_r$ is as defined above in Eq. (1), and the only nonvanishing component of $\overleftrightarrow{\gamma}$ is γ_{zz}. For a time-reversal symmetric system, $\overleftrightarrow{\varepsilon}_r$ and γ_{zz} are both real [35]. Consider again modes propagating along the z direction, compared with the case where $\gamma_{zz} = 0$, introducing γ_{zz} doesn't affect the dispersions of the two transverse modes of bands 1 and 2. The only difference is that the dispersion of the longitudinal mode (i.e., band 3) is now determined by (see Supplemental Material S-I [25])

$$\varepsilon_z - \gamma_{zz}^2 = 1 - \omega_p^2/\omega^2 - \gamma_{zz}^2 = 0. \quad (4)$$

From now on, we denote the frequency at which Eq. (4) is satisfied as ω_p'. The dispersion relations for the three modes along the z direction are shown schematically in Fig. 1(e). The same as before, we use k_c to denote the value of the wave vector of the crossing point between bands 1 and 3. In Fig. 1(f), we show the dispersion in the k_x-k_y plane at $k_z = k_c$. The dispersion becomes linear along all the directions indicating the crossing point is a Weyl point. (Plots of dispersion relations along other directions can be found in the Supplemental Material Figs. S1(a)–(c) [25].) Comparing Figs. 1(d) and 1(f), we see that the introduction of the chiral coupling drastically changes the dispersion relation. In Fig. 1(d), without the chiral coupling, the dispersion is quadratic along the y direction, i.e., $\omega - \omega_p' \propto k_y^2$ around the crossing point. Whereas with the chiral coupling the dispersion becomes $\omega - \omega_p' \propto \gamma_{zz} k_y$, as shown in Fig. 1(f); a detailed derivation of these results can be seen in the Supplemental Material S-I [25].

We can also obtain the effective Hamiltonian around this Weyl point as (See Supplemental Material S-II [25])

$$H_{\text{eff}} = \frac{1}{2\sqrt{\varepsilon_x}}(\delta_{k_z}' \mathbf{I} - \sqrt{\varepsilon_x} k_x \sigma_x + \gamma_{zz} k_y \sigma_y + \delta_{k_z}' \sigma_z), \quad (5)$$

where $\delta_{k_z}' = k_z - k_c$. The charge of this Weyl point is given by $-\text{sgn}(\gamma_{zz})$. The sign of the charge of this Weyl point can also be verified numerically; see Supplemental Material S-IV [25]. The other crossing point with a smaller k_z value in the positive half k_z space at $k_z = \sqrt{\mu\varepsilon_y}\omega_p'/c$ is also a Weyl point with charge given by $-\text{sgn}(\gamma_{zz})$ (see Supplemental Material S-II [25]). Because of the time-reversal symmetry, the charges of the two Weyl points in the negative k_z space are also $-\text{sgn}(\gamma_{zz})$. Therefore, the total charge of the Weyl points in this system is not zero. From the result above we see that the topological behavior of a uniform system can be distinctively different from that of a periodic system, such as photonic and phononic crystal systems. For a periodic system, the wave vector space is compact. Consequently, the total charge of all the Weyl points inside the first Brillouin zone must vanish [36]. On the other hand, for a uniform system, the wave vector space is not compact, and there is no longer such a constraint on the total charge.

There exist many other choices of effective parameters for which the systems also exhibit Weyl points. For example, one can have a Weyl point even when γ_{zz} is dispersive; see the Supplemental Material S-V [25]. Also, one can have Weyl points in systems that are isotropic in the x-y plane, but have chiral coupling on all three directions [25]. The results here point to substantial opportunities for exploring Weyl point physics in a wide range of reciprocal chiral metamaterials.

Types of Weyl points and relation with nonlocal effect.—In the system above, one of the two bands forming the Weyl point is flat along the z direction. The system therefore lays at the boundary that separates the phase spaces of systems exhibiting type-I and type-II Weyl points. Starting from the system discussed above, one can generate either a type-I or type-II Weyl point using the nonlocal effect that is widely known in metamaterials [20,21]. As an illustration, we assume a nonlocal ε_z that depends only on k_z:

$$\varepsilon_z = 1 - \omega_p'^2/\omega^2 + \gamma_{zz}^2 + \alpha k_z^2, \quad (6)$$

where we do a Taylor expansion in terms of k_z and keep the lowest order in k_z as allowed by time-reversal symmetry. The inclusion of higher order terms in the Taylor expansion typically only serves to shift the frequency of the Weyl point without affecting the physics here. All other parameters are the same as in Eqs. (1) and (3). When $\alpha = 0.5 > 0$, the dispersion of the longitudinal mode tilts downward generating a type-I Weyl point [Fig. 2(a)]. Whereas when $\alpha = -0.1 < 0$, the dispersion tilts upward, generating a type-II Weyl point [Fig. 2(d)]. Figures 2(b) and 2(e) [2(c) and 2(f)] show the band dispersion in the k_x-k_y (k_y-k_z) plane at $k_z = k_c$ ($k_x = 0$) for $\alpha = 0.5$ and $\alpha = -0.1$, respectively. They all possess conical structures around the crossing points between band 1 and band 3. Dispersion along other directions can be found in the Supplemental Material Fig. S1 [25]. We also note that while the type of the Weyl point changes, the charge of a Weyl point does not change as α varies.

Physical realization.—As a physical realization of the dielectric function as discussed above, we consider the structure shown in the inset in Fig. 3(a) consisting of a square lattice array of metal wires, each forming an elliptical helix. The axis of the metallic wire helix is along the z axis. The wires provide both an effective plasmonic response as well as nonlocality for ε_z. The elliptical shape of the helix provides an anisotropic dielectric response in the x-y plane. Such a system in fact has magnetic response as well with an anisotropic permeability tensor [37], which, however, does not affect the existence of a Weyl point in this system; see the Supplemental Material S-I [25]. In

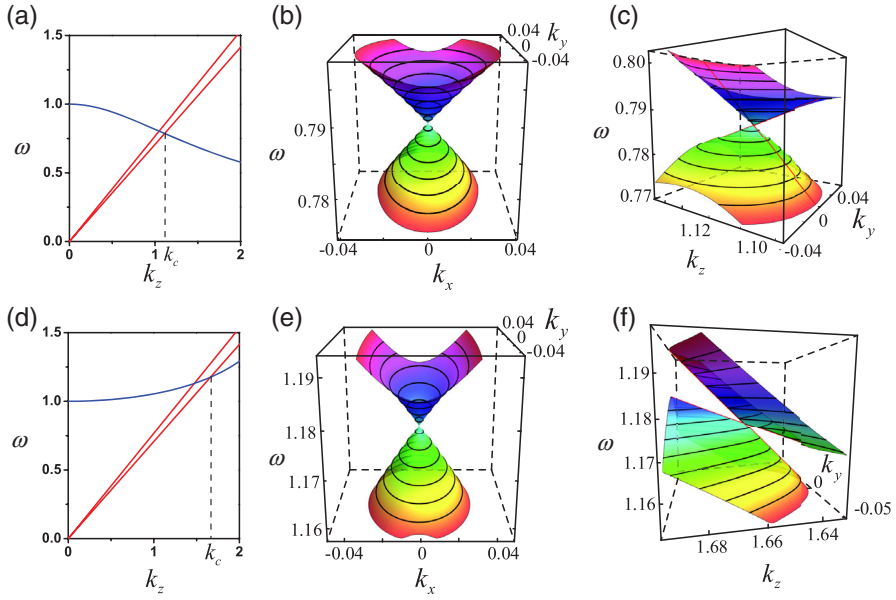

FIG. 2. (a) and (d) The dispersion along the z direction, where the red lines and blue line correspond to the transverse modes and longitudinal mode, respectively. (b) and (e) The dispersions in the k_x-k_y plane at $k_z = k_c$. (c) and (f) The dispersions in the k_y-k_z plane at $k_x = 0$. (b),(c),(e), and (f) all possess conical dispersion. The difference between type-I and type-II Weyl points can be seen by comparing (c) and (f). The parameters used here are $\omega_p' = 1$, $\varepsilon_x = 2$, $\varepsilon_y = 1.7$, and $\varepsilon_z = 1 - \omega_p'^2/\omega^2 + \gamma_{zz}^2 + \alpha k_z^2$. $\alpha = 0.5$, $\gamma_{zz} = 1.0$ for (a),(b), and (c), and $\alpha = -0.1$, $\gamma_{zz} = 0.71$ for (d),(e), and (f). The Weyl point is of type-I when $\alpha > 0$ and type-II when $\alpha < 0$. Here ω is in unit of ω_p', and the corresponding wave vectors are in unit of ω_p'/c, where c is the speed of light in the vacuum.

Figs. 3(a) and 3(b), the circles show the band structures of such an elliptical helix array with full wave simulation. Figure 3(a) shows the dispersion along the z direction, which consists of two quasitransverse modes (red) and one

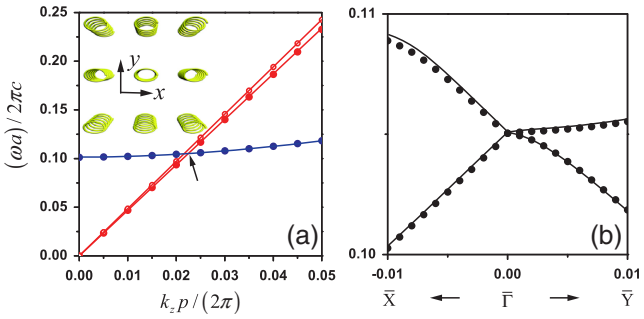

FIG. 3. (a) The band structure along the z direction with structure shown in the inset. The length of one pitch, the radius of the metallic wire, the long axis and the short axis of the helix are given by $p = 0.2a$, $\delta = 0.01a$, $\rho_x = 0.2a$, and $\rho_y = 0.1a$, respectively, where a is the lattice constant. (b) The band structure along the x and y directions around the crossing point with larger k_z as indicated by a black arrow in (a). In (a) and (b), lines are calculated with effective medium theory and circles are calculated with Comsol 5.1 and the metal is assumed to be a perfect electric conductor. The bands are linear along all the directions near the crossing point [indicated by the black arrow in (a)]. The slopes of the two bands have the same sign along k_z, but have opposite signs along k_x and k_y, indicating that it is a type-II Weyl point.

quasilongitudinal mode (blue). The quasilongitudinal mode tilts upward and hence the Weyl points here are of type II. Figure 3(b) shows the dispersion along the x and y directions around the crossing point between band 1 and band 3. The band dispersions are linear along all three directions around the crossing point. With the parameters chosen for the structure in Fig. 3, the frequency of the Weyl points here are around $0.1\ c/a$, where a is the lattice constant and c is the speed of light in vacuum, and hence the Weyl points lie in the homogenization limit where the metamaterial can be well described by homogenous effective parameters. Indeed, we can also calculate the band dispersions with the effective medium theory [37,38], (The details of this effective medium theory are provided in the Supplemental Material S-V [25].) and the results are also shown in Figs. 3(a) and 3(b) with solid lines. The band dispersions obtained through effective medium theory agrees well with the full wave simulation, indicating that this system can be well described with those effective parameters.

When a bulk system with Weyl points is truncated, if the Weyl points are located at different positions in the surface Brillouin zone, the surface supports one-way surface states that connect these Weyl points. Real metamaterials are in fact periodic structures. For a periodic structure, it is known that the total charge of the Weyl point must vanish [36]. In the metamaterial system, since in the homogenization region (i.e., the low frequency region), the total charge does not vanish, as we have shown before, the

corresponding Weyl points with opposite charges must lie outside the homogenization region with higher frequencies. Therefore, the surface states should span a much wider range of frequency, as compared to a typical photonic crystal system.

Summary and outlook.—Our work here points to the possibility for the exploration of Weyl point physics in reciprocal metamaterial systems. The relatively simple design of the structures can certainly be achieved in the microwave frequency range. Moreover, chiral metamaterial has been constructed in the midinfrared wavelength range where the properties of metals can be reasonably approximated by the perfect electric conductor model that we assume here [39,40]; thus, the physics here can be realized in the optical frequency regime as well. Given the importance of metamaterial in both fundamental physics and in device applications, the introduction of Weyl point physics into metamaterials will significantly enrich the fields of topological physics as well as metamaterials, leading to new potentials for the manipulation of electromagnetic and optical waves.

This work is supported by the U.S. Air Force of Scientific Research (Grant No. FA9550-12-1-0471). Q. L. also acknowledges the support of a Stanford Graduate Fellowship. M. X. thanks M. G. Silveirinha for helpful discussions on the effective-medium theory of the helix array.

*Corresponding author.
shanhui@stanford.edu

[1] W. Hermann, Z. Phys. **56**, 330 (1929).
[2] X. Wan, A. M. Turner, A. Vishwanath, and S. Y. Savrasov, Phys. Rev. B **83**, 205101 (2011).
[3] Z. Fang *et al.*, Science **302**, 92 (2003).
[4] B. A. Bernevig, Nat. Phys. **11**, 698 (2015).
[5] S.-Y. Xu *et al.*, Science **349**, 613 (2015).
[6] B. Q. Lv *et al.*, Phys. Rev. X **5**, 031013 (2015).
[7] B. Q. Lv *et al.*, Nat. Phys. **11**, 724 (2015).
[8] S.-Y. Xu *et al.*, Nat. Phys. **11**, 748 (2015).
[9] K.-Y. Yang, Y.-M. Lu, and Y. Ran, Phys. Rev. B **84**, 075129 (2011).
[10] A. A. Soluyanov, D. Gresch, Z. Wang, Q. Wu, M. Troyer, X. Dai, and B. A. Bernevig, Nature (London) **527**, 495 (2015).
[11] L. Lu, L. Fu, J. D. Joannopoulos, and M. Soljačić, Nat. Photonics **7**, 294 (2013).
[12] L. Wang, S.-K. Jian, and H. Yao, Phys. Rev. A **93**, 061801 (2016).
[13] J. Bravo-Abad, L. Lu, L. Fu, H. Buljan, and M. Soljačić, 2D Mater. **2**, 034013 (2015).
[14] L. Lu, Z. Wang, D. Ye, L. Ran, L. Fu, J. D. Joannopoulos, and M. Soljačić, Science **349**, 622 (2015).
[15] W.-J. Chen, M. Xiao, and C. T. Chan, arXiv:1512.04681.
[16] W. Gao, B. Yang, M. Lawrence, F. Fang, B. Béri, and S. Zhang, arXiv:1511.04875.
[17] M. Xiao, W.-J. Chen, W.-Y. He, and C. T. Chan, Nat. Phys. **11**, 920 (2015).
[18] Z. Yang and B. Zhang, arXiv:1601.07966.
[19] Y. Xu, F. Zhang, and C. Zhang, Phys. Rev. Lett. **115**, 265304 (2015).
[20] G. S. Agarwal, D. N. Pattanayak, and E. Wolf, Phys. Rev. B **10**, 1447 (1974).
[21] P. A. Belov, R. Marqués, S. I. Maslovski, I. S. Nefedov, M. G. Silveirinha, C. R. Simovski, and S. A. Tretyakov, Phys. Rev. B **67**, 113103 (2003).
[22] A. Poddubny, I. Iorsh, P. Belov, and Y. Kivshar, Nat. Photonics **7**, 948 (2013).
[23] W. Gao, M. Lawrence, B. Yang, F. Liu, F. Fang, B. Béri, J. Li, and S. Zhang, Phys. Rev. Lett. **114**, 037402 (2015).
[24] M. G. Silveirinha, Phys. Rev. B **92**, 125153 (2015).
[25] See Supplemental Material at http://link.aps.org/supplemental/10.1103/PhysRevLett.117.057401, which includes Refs. [26–32], for a detailed description of local chiral metamaterials and nonlocal metamaterials, numerical calculation of Berry phase, the effective medium theory for the metamaterial structure shown in Fig. 3a, and another example of homogeneous medium with Weyl points.
[26] K. Sun, W. V. Liu, A. Hemmerich, and S. Das Sarma, Nat. Phys. **8**, 67 (2012).
[27] S. Raghu and F. D. M. Haldane, Phys. Rev. A **78**, 033834 (2008).
[28] A. Raman and S. Fan, Phys. Rev. Lett. **104**, 087401 (2010).
[29] S. Tretyakov, I. Nefedov, A. Sihvola, S. Maslovski, and C. Simovski, J. Electromagn. Waves Appl. **17**, 695 (2003).
[30] R. Raffaele, J. Phys. Condens. Matter **12**, R107 (2000).
[31] T. A. Morgado, J. T. Costa, and M. G. Silveirinha, Phys. Rev. B **93**, 075102 (2016).
[32] A. M. Tiago, I. M. Stanislav, and M. G. Silveirinha, New J. Phys. **14**, 063002 (2012).
[33] J. B. Pendry, Science **306**, 1353 (2004).
[34] C. Wu, H. Li, Z. Wei, X. Yu, and C. T. Chan, Phys. Rev. Lett. **105**, 247401 (2010).
[35] A. H. Sihvola, A. J. Viitanen, I. V. Lindell, and S. A. Tretyakov, *Electromagnetic Waves in Chiral and Bi-Isotropic Media* (Artech House Antenna Library, Artech Print on Demand, 1994).
[36] H. B. Nielsen and M. Ninomiya, Nucl. Phys. **B193**, 173 (1981).
[37] M. G. Silveirinha, IEEE Trans. Antennas Propag. **56**, 390 (2008).
[38] M. G. Silveirinha, Phys. Rev. B **75**, 115104 (2007).
[39] J. K. Gansel, M. Thiel, M. S. Rill, M. Decker, K. Bade, V. Saile, G. von Freymann, S. Linden, and M. Wegener, Science **325**, 1513 (2009).
[40] C. M. Soukoulis and M. Wegener, Nat. Photonics **5**, 523 (2011).